

Review

Radio Galaxies—The TeV Challenge

Bindu Rani [†]

NASA Goddard Space Flight Center, Greenbelt, MD 20771, USA; bindu.rani@nasa.gov

[†] NPP Fellow.

Received: 1 November 2018; Accepted: 15 January 2019; Published: 22 January 2019



Abstract: Over the past decade, our knowledge of the γ -ray sky has been revolutionized by ground- and space-based observatories by detecting photons up to several hundreds of tera-electron volt (TeV) energies. A major population of the γ -ray bright objects are active galactic nuclei (AGN) with their relativistic jets pointed along our line-of-sight. Gamma-ray emission is also detected from nearby misaligned AGN such as radio galaxies. While the TeV-detected radio galaxies (*TeVRad*) only form a small fraction of the γ -ray detected AGN, their multi-wavelength study offers a unique opportunity to probe and pinpoint the high-energy emission processes and sites. Even in the absence of substantial Doppler beaming *TeVRad* are extremely bright objects in the TeV sky (luminosities detected up to 10^{45} erg s⁻¹), and exhibit flux variations on timescales shorter than the event-horizon scales (flux doubling timescale less than 5 min). Thanks to the recent advancement in the imaging capabilities of high-resolution radio interferometry (millimeter very long baseline interferometry, mm-VLBI), one can probe the scales down to less than 10 gravitational radii in *TeVRad*, making it possible not only to test jet launching models but also to pinpoint the high-energy emission sites and to unravel the emission mechanisms. This review provides an overview of the high-energy observations of *TeVRad* with a focus on the emitting sites and radiation processes. Some recent approaches in simulations are also sketched. Observations by the near-future facilities like Cherenkov Telescope Array, short millimeter-VLBI, and high-energy polarimetry instruments will be crucial for discriminating the competing high-energy emission models.

Keywords: active galactic nuclei; radio galaxies; gamma-rays; jets

1. Introduction

An exciting discovery enabled by space- and ground-based high-energy observations is the detection of γ -rays from over 3000 extragalactic sources. Active galactic nuclei (AGN, powered by accretion onto a few million to several billion solar mass black holes) form a major population of the γ -ray sky. AGN often produce collimated outflows, called relativistic jets (see Figure 1), whose beams of radiation pierce through the Universe and reach us from the past, offering a unique opportunity to study the Universe when it was an order of magnitude younger than today. Despite the intensive study of AGN, the location and origin of their γ -rays remains a mystery. Some studies imply the emission region is located close to the central black hole [1–5], while there are counterexamples which argue for γ -rays coming from farther out in the jet [6–8]. Extremely bright γ -ray flashes in AGN on time scales of minutes to hours have attracted the attention of the entire astronomical community, as this suggests that the particles that produce γ -rays can be accelerated with enormous efficiency in tiny regions within more extended sources. The question of what powers γ -ray AGN flares is ultimately related to the energy dissipation mechanism at work in their relativistic jets.

AGN jets are among the largest and most efficient particle accelerators in the Universe. However, where and how these particles produce high-energy radiation is still an open question. What are the particle acceleration processes, which type of particles are the primary energy drivers, and what are the high-energy interaction processes are key puzzles in high-energy astrophysics?

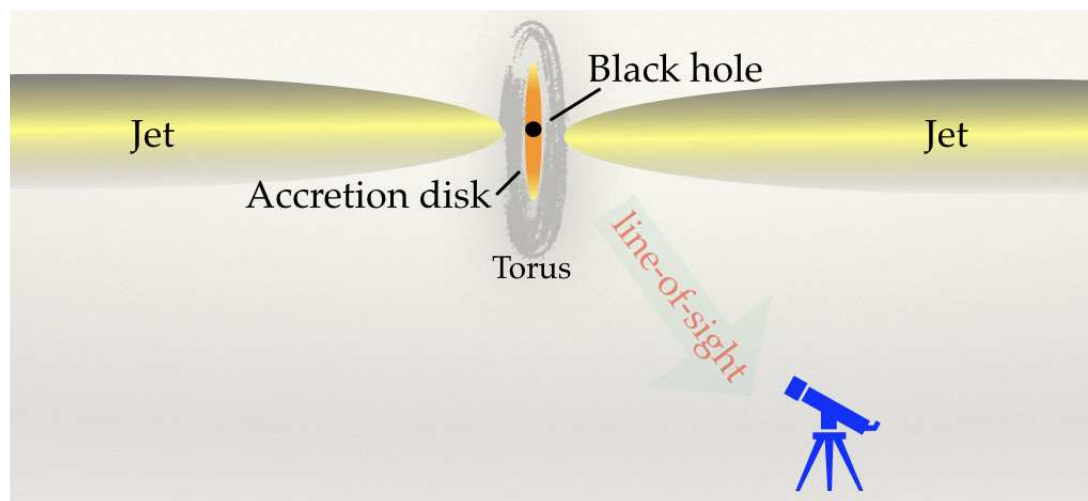


Figure 1. Sketch representing the mis-aligned radio emitting bipolar jets of a radio galaxy (not to scale). Jets typically extend up to a few hundreds of kilo-parsec to mega-parsec scales.

AGN having their jets pointed along our line-of-sight, called blazars, are the majority of the sources detected by the high-energy ground- and space-based telescopes. This goes along with the substantial Doppler boosting of their intrinsic emission. The radiation is beamed in our direction making these sources appear to be extremely bright and detectable even at larger redshifts. Blazars come in two flavors: BL Lacertae objects (BL Lacs) and flat spectrum radio quasars (FSRQs). In spite of the dissimilarity of their optical spectra—FSRQs show strong broad emission lines, while BL Lacs have only weak or no emission lines in their optical spectra—they share the same peculiar continuum properties (strong variability and high polarization). Most of the radiation we observe from these blazars is dominated by emission from the jet; however, characteristic signatures of emission from the immediate vicinity of the central black hole (accretion disk or corona) have also been observed, especially in FSRQs.

The radio to optical emission (and X-rays in some cases) from blazars is mostly synchrotron radiation from the jet, produced by relativistic electrons interacting with the jet's magnetic field. High-energy emission, which often dominates the spectral energy distribution (SED), is from inverse-Compton scattering of thermal photons (from the accretion disk, the broad-line region, or the molecular torus) and/or non-thermal photons (synchrotron emission from the jet) by the jet's relativistic electrons in case of leptonic models [1,9–12]. Gamma-ray emission could also be produced via photo-hadron interactions or hadron-nucleon (or proton-proton) collisions and subsequent cascades in the framework of hadronic models [9,12–14]. Detailed investigations of multi-wavelength flux and spectral variability of individual sources including cross-band (radio, optical, X-ray, γ -ray, and polarization), relative timing analysis of outbursts, and/or very long baseline interferometry (VLBI) component ejection/kinematics suggest that high-energy emission, especially γ rays, are associated with the compact regions of relativistic jets energized by the central SMBHs (e.g., [1,2,6,15–22]). However, many critical details of particle acceleration mechanisms and radiation processes are still unknown.

Misaligned or non-blazar AGN, such as radio galaxies or Narrow line Seyfert 1 galaxies, although representing a small fraction (<2%, [23]) of the γ -ray detected sources, have emerged as an interesting class of γ -ray emitting AGN. Radio galaxies are a particularly interesting class of objects to understand several aspects of AGN physics and high-energy emission, i.e., how the relativistic outflows are launched and driven, what drives the particle acceleration, and how and where high-energy emission is produced in jets. Several of these key questions can be addressed via studying the *TeVRad*. This review paper summarizes the key observations of *TeVRad*, with an overview about the possible particle acceleration processes and emission mechanisms, and concentrates on the jet structure and

multi-wavelength variability rather than spectral modeling, which is a separate topic. The interested reader is referred to the review article by Rieger and Levinson [24].

2. Observations of the TeV Emitting Radio Galaxies

Among the more than 30 radio galaxies observed by the *Fermi*/Large Area Telescope (LAT) reported in the LAT 8-year Point Source List (FL8Y: <https://fermi.gsfc.nasa.gov/ssc/data/access/lat/fl8y/>), six have also been detected at TeV energies (see Table 1). Most of these sources are relatively nearby; the closest is Centaurus A at a distance of 3.7 mega-parsec, while PKS 0625-35 (The source class for PKS 0625-35 is still under debate. The large-scale morphology of the source looks like that of radio galaxies, while its optical spectrum indicates a BL Lac classification [25].) at 220 mega-parsec distance is the farthest TeV-detected radio galaxy. The *TeVRad*, M87 and PKS 0625-35 have a black hole mass of a few $10^9 M_{\odot}$, which is similar to the average black hole mass of beamed radio galaxies a.k.a. blazars [26]. The other *TeVRad* host a smaller black hole, ($M_{BH} = \text{a few} \times 10^8 M_{\odot}$). The radio morphology of these sources resemble blazars when viewed at larger angles. The beaming effects are fairly moderate in *TeVRad* (apparent speed less than a few times the speed of light [27–29]).

Table 1. Radio galaxies detected at TeV energies.

Source	Type	Redshift (Distance in Mpc)	M_{BH} (M_{\odot})	L_{VHE} (erg s^{-1})
Centaurus A	FR1	0.00183 (3.7) [30]	5×10^7 [31]	10^{40}
M87	FR1	0.0044 (16) [32]	6×10^9 [33]	10^{41}
3C 84	FR1	0.0177 (71) [34]	$(3-8) \times 10^8$ [35,36]	10^{45}
IC 310	FR1	0.0189 (80) [37]	$(1-7) \times 10^8$ [31,38]	10^{44}
3C 264	FR1	0.0217 (95) [39]	2.6×10^8 [40]	6×10^{43}
PKS 0625-35	FR1/BL Lac	0.05488 (220) [41]	3×10^9 [31]	5×10^{41}

The detection of the nearest *TeVRad*, Centaurus A core, at TeV energies was first reported by H.E.S.S. (High Energy Stereoscopic System) using more than 100 h of observations taken during 2004–2006 [42]. The source has been later detected also at GeV energies by the *Fermi*/LAT [43]. *Fermi*/LAT also discovered the spatial extension in the source, detecting γ -rays from both the core and from the extended giant lobes [43]. The combined GeV-TeV spectrum of the source shows a clear excess at TeV energies and cannot be fitted via a single zone emission model [44]. Moreover, the origin of the extended γ -ray emission still remains an open question, although several models were proposed, i.e., inverse-Compton scattering of relic radiation from the cosmic microwave background and the infrared-to-optical extragalactic background light [43].

At a distance of ~ 16 Mpc, M87 was the first TeV detected radio galaxy [45]. M87 is the brightest galaxy in the Virgo cluster. The source has been detected on several occasions both in flaring and quiescent states [46–48]. The fastest variability timescale observed in the source is ~ 1 day [48]. Long-term variability on a few week timescales has also been reported for the source especially during quiescent states [47,49].

The *Fermi* telescope has detected 3C 84 since the beginning of its operation [50]. *Fermi* observations suggest that the GeV photon flux of the source has been continuously rising since then (see Section 4 for details). In 2009, the source was also detected at TeV energies [51,52]. In the end of 2016 and early 2017, the source has been through a dramatic flaring activity. During this epoch, the MAGIC telescopes detected the brightest flare ever observed in the source ($L_{\gamma\text{-ray}} \sim 10^{45} \text{ erg s}^{-1}$, [4]) with a flux doubling timescale of ~ 10 h.

The radio galaxy IC 310 was first detected at TeV energies in 2009–2010 by the MAGIC telescope [53]. Variations on days to months timescales were observed in the source during this period. On 12–13 November 2012, a dramatic flare was observed in the source. During this exceptional variability phase, the observed flux doubling timescale of the observed TeV flares was as short as 5 min. This is the fastest variability timescale observed in a radio galaxy up to now [38]. This extreme

flare is quite challenging to be explained within the framework of any existing theoretical mechanism (see Section 6 for details).

At a distance of 95 Mpc, 3C 264 is rather a new member in the family. Nearly 12 h of VERITAS observations of the source between 9 February 2018 and 16 March 2018 confirms its detection at $\sim 5\sigma$ level [54]. TeV emission above 250 GeV from PKS 0625-35 was first reported in 2012 by H.E.S.S. [55]. *Fermi* observations of the source report variations on monthly timescales [56]. However, no variation has been seen at TeV energies. The source belongs to the category of low excitation line radio-loud AGN [57]. Radio observations find superluminal motion in the jet with apparent speeds up to $\sim 3c$ [58]. The evidence of a one-sided jet and superluminal motion suggests the source to be more like a blazar.

3. Radio Properties

3.1. Parent Population

All *TeVRad* are Fanaroff and Riley type I (FR1) sources. Moreover, most of the TeV-detected blazars (high-frequency peaked BL Lacs, HBL, in TeVcat: <http://tevcap.uchicago.edu/>) belong to the parent population of FR1 sources. Radio galaxies are classified as FR1 and FR2 [59] sources on the basis of their jet luminosity at 178 MHz radio frequency. It was found that the sources with luminosity $\geq 5 \times 10^{24} \text{ W Hz}^{-1} \text{ Sr}^{-1}$ belong to the FR2 class, while the rest were classified as FR1 type [59]. The key difference between the two populations is their radio morphology. FR2s are more powerful radio galaxies, and their radio morphology is characterized by powerful edge-brightened double lobes with prominent hot spots, while the FR1s are lower-power sources, which exhibit rather diffuse edge-darkened lobes. Moreover, FR2s tend to be found in less dense environments compared to FR1s. When seen at small inclinations, FR1 sources are BL Lacs while FR2s are radio-loud quasars (an excellent discussion about AGN unification can be found in Urry and Padovani [60]).

It was found that at a given radio power, FR1s have fainter nuclear X-ray and ultra-violet (UV) emission [61,62] compared to FR2s, which indicates that FR1s might have fainter accretion disks. For instance, the accretion rate for the brightest *TeVRad* 3C 84 ($L_{VHE} = 10^{45} \text{ erg s}^{-1}$) is well below 10% of its Eddington accretion rate (Eddington ratio $\sim 3 \times 10^{-4}$, [63]). The key question to answer is if this corresponds to different accretion modes in the two classes of sources [64]. If yes, it would be interesting to assess how it correlates to their observed TeV luminosity. Moreover, FR2s may occupy less dense environments, enabling lower $\gamma\gamma$ -pair production opacity for the TeV photons. In dense environments, high-energy photons might get absorbed via a process called pair production when they interact with lower-energy (optical/UV) photons by producing electron–positron pairs.

3.2. Jet Kinematics—Speeds on Parsec to Kilo-Parsec Scales

The *TeVRad* M87 is the best studied radio galaxy because of its extremely bright and spectacular jet extending up to several hundreds of kilo-parsecs. Figure 2 depicts the kilo-parsec scale radio, optical, and X-ray images (from top to bottom) of the M87 jet. The high-resolution VLBI observations show very sub-luminal speeds ($\sim 0.01c$) on tens of parsec scales [28,65,66], although recent higher-cadence VLBI monitoring programs have started to find faster motions at the similar scales [67,68]. Later, there is a sudden increase in the apparent speeds at a distance of ~ 100 parsecs close to the location of HST-1 feature (see Figure 3). Superluminal components with speeds up to $6c$ are detected after that (see Figure 3), which is followed by a smooth deceleration [69–71]. A similar velocity pattern has been observed in 3C 264. The sub-luminal apparent speeds ($\leq 0.5c$) seemingly receive a kick at a distance of ~ 100 parsec where the jet has a stationary knot/feature. On kilo-parsec scales apparent speeds up to $7c$ have been observed in the source [29]. Downstream acceleration with a change in speeds from 0.1 – 0.3 to $0.5c$ has also been observed in the kilo-parsec scale jet of Centaurus A [72–74]. How exactly these velocity fields develop and evolve along the jet is still an open issue. The stationary features are thought to be the sites of recollimation shocks, which might have a key role in accelerating the sub-luminal motion to super-luminal speeds.

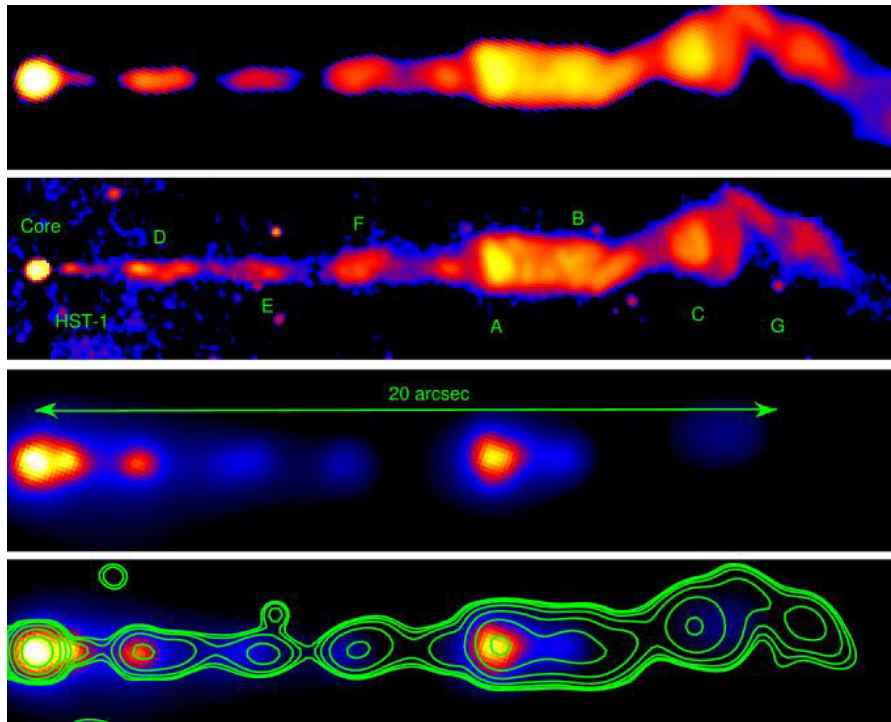


Figure 2. Multi-wavelength view of the M87 jet. From top to bottom: radio jet imaged by Very Large Array (VLA), optical jet seen by the Hubble Space Telescope, and X-ray image taken by the Chandra X-ray Observatory. The optical image (middle) marks the position of various bright knots/stationary features observed in the jet. (Credit: Marshall et al. [75], reproduced with permission ©AAS).

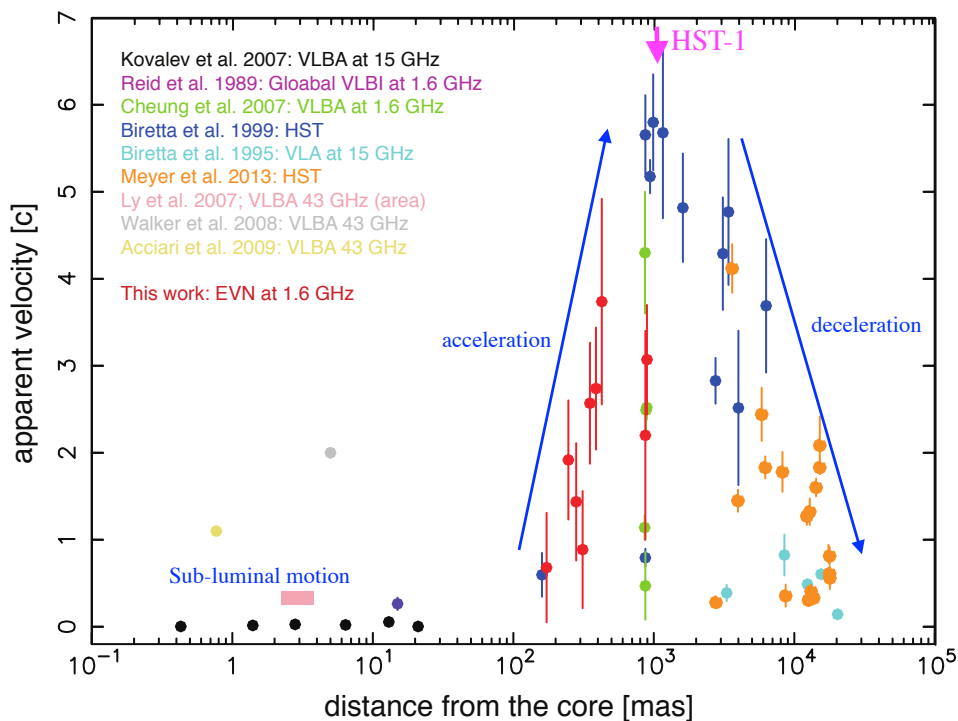


Figure 3. Velocity field measurements in the jet of M87 from parsec to kilo-parsec scales. The stationary feature HST-1 is at a distance of ~ 100 parsecs from the central engine. The highest speeds are measured close to the position of HST-1. (Credit: Asada et al. [65], reproduced with permission ©AAS).

There has been no dramatic change noticed in the apparent speed of the moving features in the other *TeVRad* as a function of distance from the central engine. For instance, the observed speeds on parsec and kilo-parsec scales are sub-luminal ($\sim 0.2\text{--}0.9 c$) in 3C 84 [8,76–78], suggesting a viewing angle $\geq 45^\circ$. The one-sided blazar like jet of IC 310 constrains the viewing angle to be $\leq 38^\circ$ implying a moderate beaming [79]. VLBI observations measure an apparent speed of $\sim 0.9\text{--}3 c$ in the PKS 0625-35 jet, which constrains the viewing angle in the source to be $\leq 13^\circ$ (Angioni et al. 2018, submitted).

Structured and stratified velocity patterns have also been observed in the parsec-scale jets of some of the *TeVRad*. For instance, a study by Mertens et al. [28] reports a stratification in the M87 jet with three different velocity patterns. The jet flow in the source has a slow, mildly relativistic layer, sheath, (apparent velocity $\sim 0.5 c$) and a fast spine (apparent velocity $\sim 0.9 c$). The study also discovered a significant difference in the apparent speeds observed in the northern ($0.5 c$) and southern ($0.2 c$) limbs of the jet (the bright limbs in the source can be seen in Figure 4). Likewise, limb brightening was discovered in the 3C 84 jet using the space-VLBI observations [80]. Hints of differential motion were also observed in Centaurus A [72].

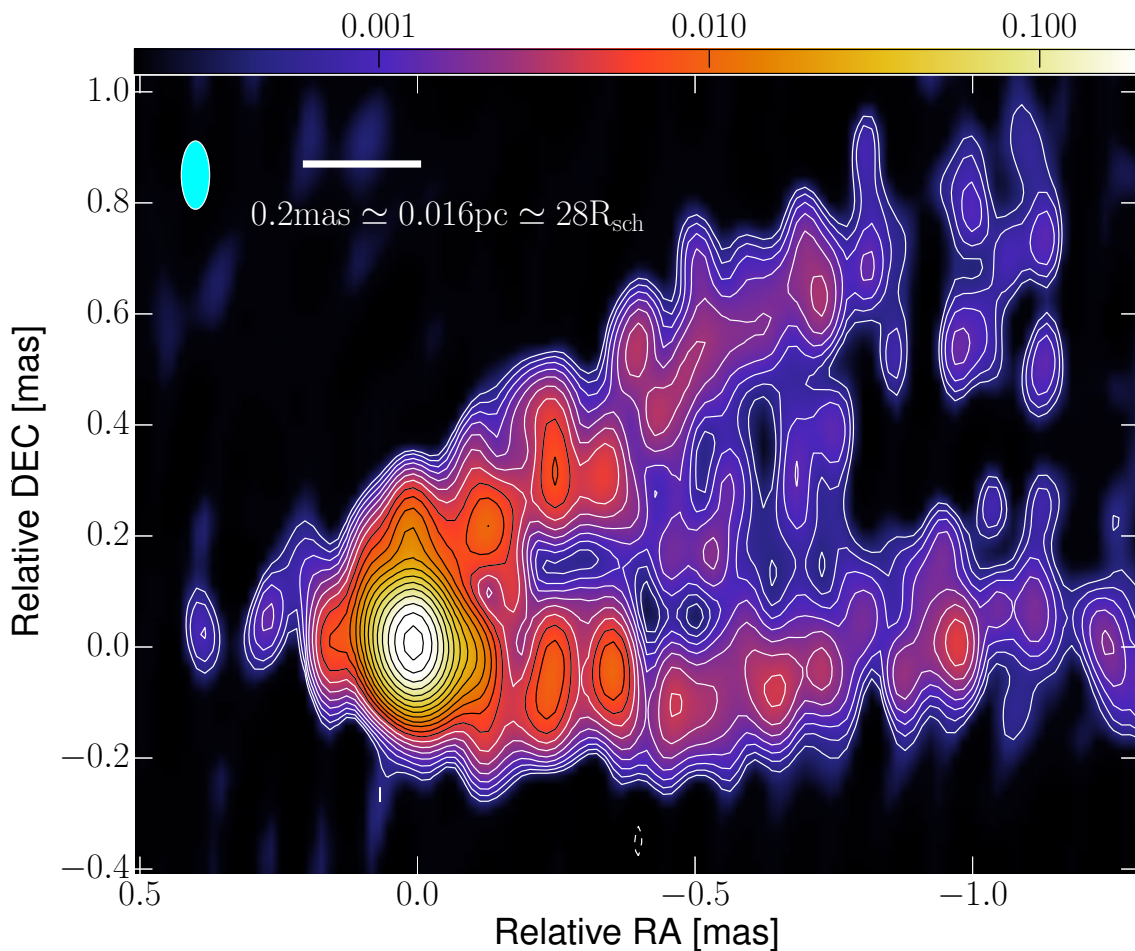


Figure 4. Stacked high-resolution radio image of M87 at 86 GHz frequency (Credit: Kim et al. [81], reproduced with permission ©ESO). The high-resolution radio imaging technique allows a zoom up to a scale of ≤ 10 gravitational radii in the source frame.

3.3. Zooming into the Event Horizon Scales

AGN jets are the most spectacular structures in the Universe and represent the “extreme” and “largest” members of a wide family of jet-powered phenomena, including γ -ray bursts (GRBs), X-ray binaries (XRBs), and young stellar objects (YSOs). Over the past few decades, there has

been remarkable progress in our understanding of AGN jet physics especially because of the development of high-resolution VLBI (for more details refer to the recent review on millimeter-VLBI by Boccardi et al. [82]). Millimeter-VLBI observations offer an angular resolution of a few tens of micro-arcseconds, which allows a probe of the inner jet region on scales ≤ 50 gravitational radii (R_g).

Given its proximity and fairly bright jet at millimeter radio frequencies, M87 is the best studied source using high-resolution VLBI [28,65,81,83,84]. Global millimeter VLBI observations at 86 GHz radio frequency resolve a limb-brightened outflow down to $\sim 15 R_g$ [81,85]. A high-resolution image of M87 taken at 86 GHz radio frequency is illustrated in Figure 4. The Event Horizon Telescope (EHT) observations at 230 GHz and 345 GHz frequencies constrain the size of the event horizon of the central black hole to be less than $10 R_g$ [84,86]. These high-resolution images provided a unique tool to test the different jet-launching models [83,84].

Another interesting study is made using the space-VLBI observations. The space-VLBI observations of 3C 84 at 22 GHz radio frequency using the *RadioAstron* mission probed the inner jet profile up to $100 R_g$ [80]. The study discovered a very broad jet base with a transverse radius larger than about $250 R_g$ implying the jet to be more likely launched from the accretion disk. More interestingly, Global millimeter VLBI Array (GMVA) observations at 86 GHz radio frequency discovered a double-nuclear structure at the jet base (Oh et al. 2018, in preparation).

High-resolution VLBI observations therefore offer an unparalleled opportunity to probe and pinpoint the high-energy emitting sites in the immediate vicinity of the central black hole. Moreover, high-resolution polarization imaging is a unique technique to unravel the magnetic field topology on scales less than a few hundreds of gravitational radii. The tiny magnetized regions in the extended jets are the potential sites of high-energy emission [20,87,88].

4. TeV Variability

Like blazars, *TeVRad* exhibit variability on multiple timescales i.e., sub-hour to days timescale flares are accompanied by long-term outbursts. For instance, multiple modes of flaring activity can be seen in the γ -ray light curve of 3C 84 observed by the *Fermi*/LAT. Figure 5 presents the rapid flares superimposed on top of the long-term rising trend in the *Fermi* photon flux light curve (in blue). At the end of 2016, several extremely bright and rapid flares were observed by *Fermi*/LAT. The fastest flares seen by *Fermi*/LAT have flux doubling timescale of 9–12 h. In 2016–2017, the source was also detected multiple times at TeV energies by the MAGIC telescope (see Figure 6) [4]. During the course of this period, MAGIC detected the fastest and most luminous flare from 3C 84. An extremely bright ($L_\gamma \simeq 10^{45}$ erg s^{-1}) flare with a flux doubling timescale of ~ 10 h was observed on 1 January 2017 [4]. Flux variations on multiple timescales were also observed in IC 310 and M87.

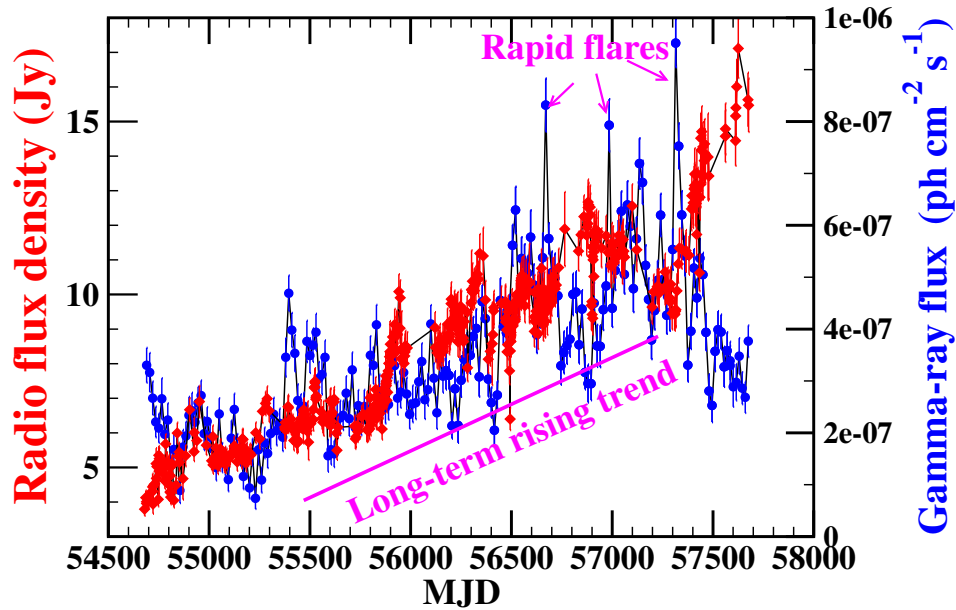


Figure 5. Gamma-ray photon flux (blue) and radio 230 GHz (red) light curve of the *TeVRad* 3C 84 at $E = 0.1\text{--}300$ GeV. The γ -ray light curve is produced by adaptive binning analysis method following Lott et al. [89] using the *Fermi*/LAT data from August 2008 until September 2017. The radio 230 GHz light curve is from sub-millimeter array (SMA) AGN monitoring program (details are referred to Hodgson et al. [8]). Rapid flares superimposed on top of the long-term rising trend can be seen both at γ -ray and radio frequencies.

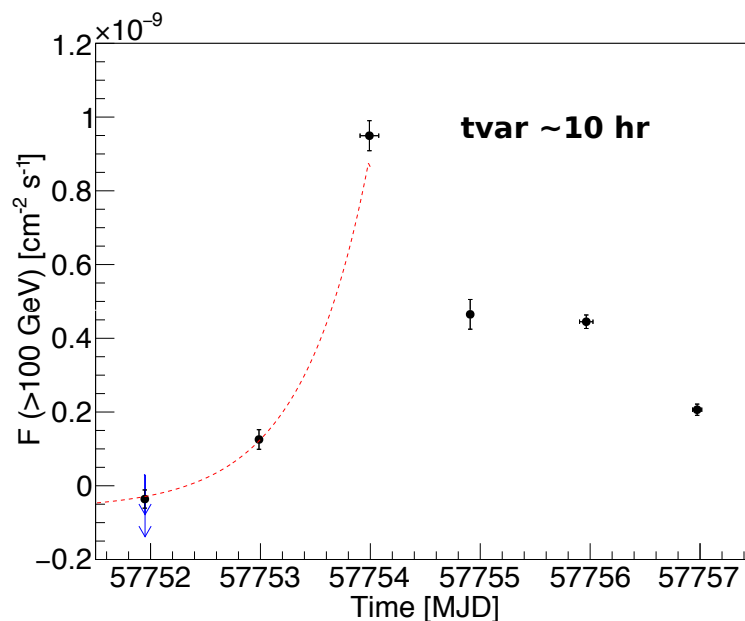


Figure 6. TeV light curve of 3C 84 observed by the MAGIC telescope [4]. The fastest flare observed around January 01, 2017 has a flux doubling timescale of ~ 10 h. Long-term variations at γ -rays are shown in Figure 5.

Extremely short variability timescales in *TeVRad* have attracted the attention of astrophysicists, as the observed timescales can reach down to the light crossing time of the black hole event horizon, $t_{BH} = r_g/c$, where r_g is the gravitational radius of the black hole and c is the speed of light. For instance, the observed variability timescale ($t_{var} = 5$ min) in IC 310 is much smaller than the event horizon light crossing timescale, $t_{BH} = 25$ min [38]. The fastest variability timescale observed in M87 ($t_{var} \sim$

1 day) is comparable with the event horizon light crossing timescale ($t_{BH} \sim 60\text{--}90$ min). Variations on sub-horizon scales have also been observed in blazars [90]. However, in case of blazars, one can always argue that beaming effects make the observed timescale appear shorter. This requires the Doppler factor to be greater than 50, which has rarely been observed [27,78].

Understanding the physical processes responsible for the origin of the ultra-fast TeV flares is a key challenge in high-energy astrophysics. Sub-horizon scale variations and extremely luminous flares, especially in the absence of strong beaming effects, require (i) emission regions of extremely high electromagnetic energy of the emitting particles, (ii) efficient particle acceleration mechanisms which could channel the electromagnetic energy to particle energy, and (iii) less-dense photon environments so that the emitted TeV photons do not get self-absorbed by $\gamma\gamma$ -pair production.

5. High-Energy Emitting Sites

Locating the γ -ray emitting sites is a key challenge not only in case of radio galaxies but also for blazars. When the emission region is closer to the central black hole, there is higher proportion of electromagnetic energy available in the jet, making it easy to account for the observed extremely bright γ -ray flashes. However, if the high-energy photons are produced too close to the black hole, the chances for them to escape through the rich photon environments are low. Nevertheless, at least some of these high-energy photons seem to survive even through dense environments. Photons produced further down in the jet have higher chances of not being absorbed; however, accelerating particles to extreme high-energy is a quite challenge there (see Section 6 for more details).

The sub-horizon scale emitting regions, detected in IC 310, 3C 84, and M87, could either be very close to the black hole or further down in the jet. The TeV flare in IC 310 was interpreted as originating from the magnetospheric gap of the black hole (see Section 6) as it is hard to achieve the high luminosity and rapid variability further down in the jet. The rapid TeV flare in 3C 84 was also proposed to be produced in the magnetospheric gap; however, achieving the extremely high luminosity requires an extremely fast rotating black hole and magnetic field higher than its equipartition value [4]. However, these studies lack a conclusive observational evidence for the emission to be produced close to the black hole. Multi-frequency observations of M87 during an episode of extremely rapid flares provided an opportunity to study the TeV emitting regions in great detail. Strong TeV flares in the source were accompanied by an increase of the flux from the nucleus observed at 43 GHz radio frequency [5], suggesting the emission region to be located within the radio core (≤ 50 gravitational radii). The extreme compactness of the TeV emission region and the observed TeV-radio connection in M87 conclusively infer that the VHE emission is indeed produced very close to the black hole [5]. This scenario has further been strengthened by more recent TeV-VLBI joint observations of M87 [91,92], where the authors also found the flux increase of the 43 GHz core along with TeV flaring events.

Hints of multiple γ -ray emitting regions have also been observed in *TeVRad*. For instance, a study performed using the KVN (Korean VLBI Network) and γ -ray observations indicate the presence of multiple γ -ray emitting regions in 3C 84 [8]. Figure 5 presents a comparison of the flux variations observed at γ -ray and 230 GHz radio frequencies. The long-term rising trend is present in the flux variations seen both at radio and γ -ray frequencies. However, the rapid flares do not have a one-to-one correspondence at the two frequencies. A formal cross-correlation analysis indicates two prominent peaks at around -500 and $+400$ days, which implies that γ -rays variations lead those at radio by -500 days and also lag behind by $+400$ days (see Figure 7). A detailed investigation of the flux density variations in the spatially separated emission regions of the jet indicates the presence of multiple γ -ray emitting sites in the source. The study reported that there are two active regions producing γ -rays in the source, one very close to the black hole and another at a distance of ~ 4 parsec in the source frame.

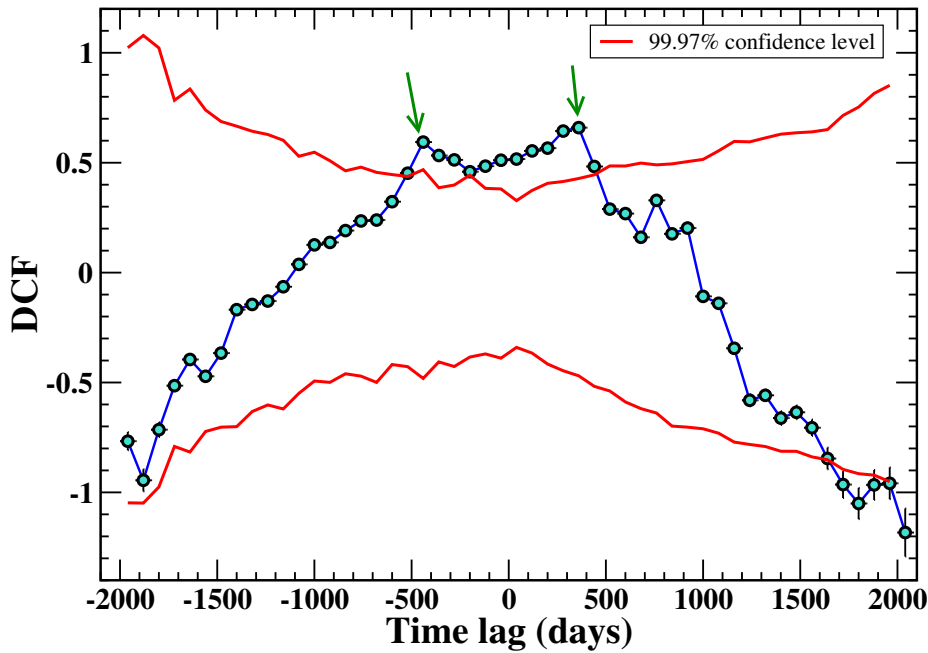


Figure 7. Cross-correlation analysis curve of the γ -ray and radio flux variations observed in 3C 84 (see Figure 5). The two peaks at -500 and $+400$ days (green arrows) imply γ -rays flux variations leading and lagging those at radio. A detailed analysis suggests the presence of multiple γ -ray emitting sites in the source [8].

Fermi has detected γ -rays both from the core and the extended lobes of the nearest *TeVRad* Centaurus A [43]. The source has a spatial extension of about 9 degrees across the sky, which corresponds to ~ 600 kilo-parsec, and the γ -ray morphology (Magill et al. 2019, in preparation) is quite similar to its radio jet morphology, which implies γ -rays coming from both the central AGN core and extended kilo-parsec scale lobes. Given the detection of extended γ -ray emission at GeV energies and the absence of TeV variability, the extension of TeV emission cannot be discarded. It is important to note that *Fermi*/LAT has detected extended GeV emission also from Fornax A. It might be interesting to see for how many of these sources spatial extension can be detected by using the future Cherenkov Telescope Array.

6. Particle Acceleration Mechanisms

The observed extremely rapid variability and enormously high γ -ray luminosity are clearly challenging to achieve in astrophysical jets as they require (i) particle acceleration to extreme high energies in the presence of strong radiative loss (ii) variation on sub-horizon timescales, and (iii) conversion of large volumes of electromagnetic energy with enormous efficiency. Several mechanisms have been proposed to address the TeV challenge in astrophysical sources. Some recent ideas are summarized below.

The most common mechanism is relativistic shock i.e., the flow is accelerated to supersonic speeds and strong shocks are formed in the relativistic outflow because of (i) faster moving outflow runs into slower flow resulting in the formation of internal shock, (ii) the outflow encounters an obstacle (perhaps a molecular cloud) on its way, (iii) any other perturbation happening at the base of the jet could also form a shock wave to form and propagate down the jet. Relativistic shocks [93] seem to be effective in low-magnetization regimes and could explain the observed long-term variability from AGN fairly well [1,20,87,88,94–96]. However, the luminous ultra-fast TeV flares observed from a number of AGN [4,38,90,97] are difficult to explain via the relativistic shock model, especially in the absence of substantial Doppler beaming, and therefore challenge our understanding of particle acceleration processes.

Magnetic reconnection, a process by which magnetic energy is transferred to particle heat, bulk energy and non-thermal energy, is proposed to be an effective mechanism for energy dissipation [98–102] in magnetically dominated relativistic outflows. During magnetic reconnection, opposite polarity magnetic field lines exchange partners at “X-points” leading to breaking of flux freezing and change in magnetic field topology, which results in an explosive release of energy. For instance, solar flares seem to be powered by magnetic reconnection. However, this picture is far too complex in case of relativistic outflows. Nevertheless, there has been great advancement in simulations to understand the relativistic magnetic reconnection. The particle-in-cell (PIC) magnetic reconnection simulations suggest that ultra-relativistic plasmoids generated by magnetic reconnection [99,100] can power the ultra-fast flares observed from TeV AGN. An example γ -ray light curve (top) and snapshot of relativistic magnetic reconnection (bottom) by an integrated modeling relying on first-principle PIC kinetic simulation and an advanced polarized radiation transfer simulation from Zhang et al. [98] are illustrated in Figure 8. The study reports that plasmoid coalescences in the magnetic reconnection layer can produce highly variable multi-wavelength light curves, and also can explain polarization degree and polarization angle variations.

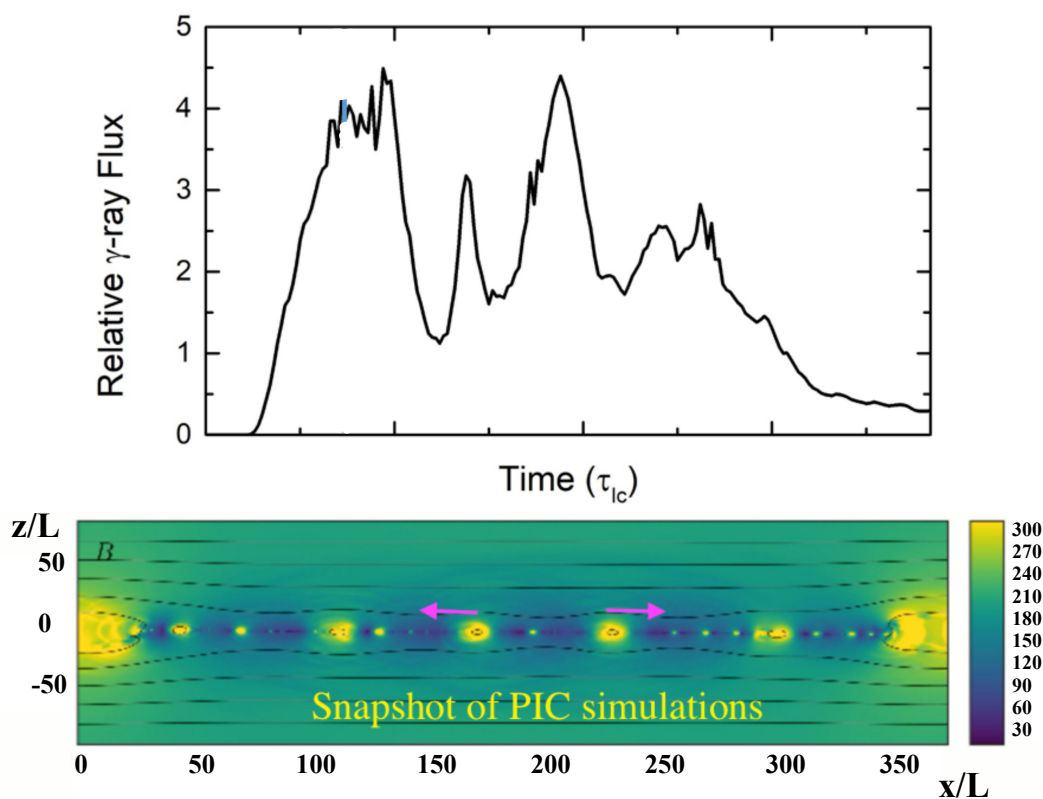


Figure 8. Radiative signatures of relativistic magnetic reconnection by an integrated modeling relying on first-principle particle-in-cell (PIC) kinetic simulation (Credit: Haocheng Zhang [98]). (Top) γ -ray light curve in units of light crossing time scale. (Bottom) reconnection layer in the unit of ion skin depth.

A magnetospheric gap model was invoked to explain the sub-horizon scale flux variations in *TeVRad* [4,38,103,104]. It has been proposed that a rotating black hole embedded in a strong magnetic field (of the order of 10^4 – 10^5 G) will induce an electric field, E , corresponding to a voltage drop across its event horizon, which facilitates an efficient electromagnetic extraction of the rotational energy of the black hole (for more details, see the review by Rieger [104]), and could be an efficient mechanism to power the TeV flares in AGN. The maximum extractable energy ($L_{magnetosphere}$) from the black hole, however, depends on the details of the gap configuration. For instance, $L_{magnetosphere}$ scales as the height

of the magnetospheric gap (h) i.e., $L_{\text{magnetosphere}} \sim L_{\text{BZ}}(h/r_g)^\beta$, where L_{BZ} is the maximum power from a fast rotating black hole [105] and β depends on the gap setup. The size of the gap can be constrained by the observed TeV variations ($c\delta t \leq r_g$), which further reduces the maximum $L_{\text{magnetosphere}}$ (details are referred to [104,106]). Another important aspect of this model is the absorption of the emitted TeV photons by the thermal photon environment of the black hole. In order for the TeV photons to survive through the accretion disk environment, the magnetospheric gap model requires an under-luminous or radiatively inefficient accretion flow to avoid $\gamma\gamma$ -pair production. This enforces accretion rates to be below 1% of the Eddington scale. Putting this in the context of current observations, the model could explain the observed TeV flares in M87 fairly well; however, the minute-scale TeV flare in IC 310 seems less likely to have a magnetospheric gap origin. The observed TeV luminosity in 3C 84 is also hard to match in the framework of the magnetospheric gap model unless the magnetic field threading the accretion disk is a factor of 1000 greater than its equipartition value.

Magnetoluminescence [107,108] has been recently proposed to explain the observed TeV flares from astrophysical sources. The basic idea is that rotating at the center of an AGN leads to writhing of magnetic flux ropes resulting in tangled and knotted magnetic field lines. The tightly wound magnetic flux ropes especially in the inner jet are highly dynamically unstable. The tangled/knotted flux lines when opened up or untangled could produce rapid γ -ray flares. It has been suggested that this phenomenon includes an implosion rather than explosion [108]. As a consequence, particles could be accelerated to significantly higher energies as the dissipating and cooling volume could be re-energized by the medium external to it. Electromagnetic detonation [108] is proposed as an alternative possibility, which might accelerate particles at the transition of high-magnetized outflow into low-magnetized outflow and energy-flux. Particles are subjected to unbalanced electric field at the transition and get accelerated (positive and negative charged particles are accelerated in opposite direction) to produce γ -rays. In comparison to magnetic reconnection, which requires a magnetic flux to channel into a small volume, electromagnetic detonation will have a larger volume for the conversion of electromagnetic energy into particle energy.

7. Future Directions

Pinpointing the sub-horizon scale γ -ray emitting sites in kilo-parsec to mega-parsec scales AGN jets is a key challenge in high-energy astrophysics. A coordinated multi-wavelength and multi-messenger effort is needed to better understand it. The TeV emitting radio galaxies (*TeVRad*) are a particularly interesting class of AGN to unravel the mystery of the origin of γ -ray emission. Some important considerations are:

- *TeVRad* are nearby AGN. The farthest detected *TeVRad* is at a distance of 220 Mpc. Using the millimeter-VLBI observations, we can probe regions in the immediate vicinity of the central black hole i.e., down to a scale of less than 50 gravitational radii in the source frame (for more details about the imaging capabilities of the current and near-future high-resolution VLBI observations, check Boccardi et al. [82]). The mm-VLBI observations will provide an ultimate opportunity to probe the compact regions closer to the black hole, which are the potential sites of high-energy emission. High-resolution polarization imaging will probe the magnetic field strength and configuration of these compact emission regions, which is an essential piece of information in order to understand the production mechanisms of high-energy emission.
- Being seen off-axis, *TeVRad* offers a unique opportunity to transversely resolve the jet. Using high-resolution VLBI, one can transversely resolve the fine scale jet structure and can probe their flux density and polarization variations. VLBI astrometry observations could provide the exact location of the core. Having that, we could combine the high-resolution VLBI imaging and multi-wavelength observations to exactly pinpoint the location of γ -ray emitting sites.
- There have been great advances in the theory and simulation front. Several details about plasma physics under extreme conditions can be better understood via simulations i.e., radiative signatures of relativistic magnetic reconnection [98–102], formation of jets and expulsion of

magnetic flux from the central black hole [109–111], high-energy polarization signatures of shocks and reconnection [98,112,113]. A comparison of predictions from simulations with measurements will be crucial to understanding the physical processes happening around black holes.

- Cherenkov Telescope Array (CTA) [114] with its sensitivity better than the existing GeV/TeV instruments and spatial resolution of the order of a couple of arc-minutes at TeV energies will provide observations up to 300 TeV. CTA will detect many more misaligned AGN and will also help us in separating nuclear and off-nuclear components especially for nearby sources. Having the potential to probe deeper into the spectral and variability characteristics of AGN, CTA will eventually revolutionize our understanding of the TeV sky.
- The question of what powers γ -ray AGN flares is ultimately related to the energy dissipation mechanism at work. High-energy polarization observations will deliver an ultimate test for probing the energetic particle-acceleration processes and emission mechanisms: (i) leptonic versus hadronic models and (ii) shocks versus magnetic reconnection. High-energy polarimetry missions are on their way to unravel how the most efficient particle accelerators in the Universe work. For instance, the All-sky Medium Energy Gamma-ray Observatory (AMEGO: <https://asd.gsfc.nasa.gov/amego/>) will offer MeV polarization observations of the γ -ray bright AGN. The Imaging X-ray Polarimetry Explorer (IXPE: <https://wwwastro.msfc.nasa.gov/ixpe/index.html>) will observe polarization signatures from X-ray bright AGN.
- The recent observations of coincidence of a high-energy neutrino event with a flaring AGN, TXS 0506+056 indicate AGN as potential sources of high-energy neutrinos [115]. Multi-wavelength and multi-messenger observations of similar events will test if AGN jets are powerful sources of extra-galactic neutrinos and put constraints on lepto-hadronic models.

Given the flood of high quality data from the current and upcoming missions and great advances in theory/simulation, it is an exciting time for astronomers. There are several major discoveries to be made.

Acknowledgments: B.R. acknowledges the help of Dave Thompson, Chris Shrader, Lorentzo Sironi, Benoit Lott, Zorawar Wadiasingh, and Alice Harding for their fruitful discussions and comments that improved the manuscript.

Funding: This research was supported by an appointment to the NASA Postdoctoral Program at the Goddard Space Flight Center, administered by Universities Space Research Association through a contract with NASA.

Conflicts of Interest: The authors declare no conflicts of interest.

References

1. Rani, B.; Krichbaum, T.P.; Fuhrmann, L.; Böttcher, M.; Lott, B.; Aller, H.D.; Aller, M.F.; Angelakis, E.; Bach, U.; Bastieri, D.; et al. Radio to gamma-ray variability study of blazar S5 0716+714. *Astron. Astrophys.* **2013**, *552*, A11. [[CrossRef](#)]
2. Rani, B.; Krichbaum, T.P.; Marscher, A.P.; Jorstad, S.G.; Hodgson, J.A.; Fuhrmann, L.; Zensus, J.A. Jet outflow and gamma-ray emission correlations in S5 0716+714. *Astron. Astrophys.* **2014**, *571*, L2. [[CrossRef](#)]
3. Algaba, J.C.; Lee, S.S.; Kim, D.W.; Rani, B.; Hodgson, J.; Kino, M.; Trippe, S.; Park, J.H.; Zhao, G.Y.; Byun, D.Y.; et al. Exploring the Variability of the Flat Spectrum Radio Source 1633+382. I. Phenomenology of the Light Curves. *Astrophys. J.* **2018**, *852*, 30. [[CrossRef](#)]
4. MAGIC Collaboration; Ansoldi, S.; Antonelli, L.A.; Arcaro, C.; Baack, D.; Babić, A.; Banerjee, B.; Bangale, P.; Barres de Almeida, U.; Barrio, J.A.; et al. Gamma-ray flaring activity of NGC 1275 in 2016–2017 measured by MAGIC. *Astron. Astrophys.* **2018**, *617*, 91.
5. Acciari, V.A.; Aliu, E.; Arlen, T.; Bautista, M.; Beilicke, M.; Benbow, W.; Bradbury, S.M.; Buckley, J.H.; Bugaev, V.; Butt, Y.; et al. Radio Imaging of the Very-High-Energy γ -Ray Emission Region in the Central Engine of a Radio Galaxy. *Science* **2009**, *325*, 444. [[PubMed](#)]
6. Agudo, I.; Jorstad, S.G.; Marscher, A.P.; Larionov, V.M.; Gómez, J.L.; Lähteenmäki, A.; Gurwell, M.; Smith, P.S.; Wiesemeyer, H.; Thum, C.; et al. Location of γ -ray Flare Emission in the Jet of the BL Lacertae Object OJ287 More than 14 pc from the Central Engine. *Astrophys. J. Lett.* **2011**, *726*, L13. [[CrossRef](#)]

7. Jorstad, S.G.; Marscher, A.P.; Smith, P.S.; Larionov, V.M.; Agudo, I.; Gurwell, M.; Wehrle, A.E.; Lähteenmäki, A.; Nikolashvili, M.G.; Schmidt, G.D.; et al. A Tight Connection between Gamma-Ray Outbursts and Parsec-scale Jet Activity in the Quasar 3C 454.3. *Astrophys. J.* **2013**, *773*, 147. [[CrossRef](#)]
8. Hodgson, J.A.; Rani, B.; Lee, S.S.; Algaba, J.C.; Kino, M.; Trippe, S.; Park, J.H.; Zhao, G.Y.; Byun, D.Y.; Kang, S.; et al. KVN observations reveal multiple γ -ray emission regions in 3C 84? *Mon. Not. R. Astron. Soc.* **2018**, *475*, 368–378. [[CrossRef](#)]
9. Böttcher, M.; Reimer, A.; Zhang, H. Leptonic and Hadronic Modeling of Fermi-Detected Blazars. Spectral Energy Distribution Modeling and High-Energy Polarization Predictions. *Eur. Phys. J. Web Conf.* **2013**, *61*, 05003. [[CrossRef](#)]
10. Böttcher, M. Modeling the emission processes in blazars. In *The Multi-Messenger Approach to High-Energy Gamma-Ray Sources*; Springer: Dordrecht, The Netherlands, 2007; pp. 95–104.
11. Rybicki, G.B.; Lightman, A.P. *Radiative Processes in Astrophysics*; Wiley: New York, NY, USA, 1986; p. 400.
12. Dermer, C.D.; Menon, G. *High Energy Radiation from Black Holes: Gamma Rays, Cosmic Rays, and Neutrinos*; Princeton University Press: Princeton, NJ, USA, 2009.
13. Zhang, H.; Böttcher, M. X-Ray and Gamma-Ray Polarization in Leptonic and Hadronic Jet Models of Blazars. *Astrophys. J.* **2013**, *774*, 18. [[CrossRef](#)]
14. De Angelis, A.; Mallamaci, M. Gamma-ray astrophysics. *Eur. Phys. J. Plus* **2018**, *133*, 324. [[CrossRef](#)]
15. Jorstad, S.G.; Marscher, A.P.; Mattox, J.R.; Aller, M.F.; Aller, H.D.; Wehrle, A.E.; Bloom, S.D. Multiepoch Very Long Baseline Array Observations of EGRET-detected Quasars and BL Lacertae Objects: Connection between Superluminal Ejections and Gamma-Ray Flares in Blazars. *Astrophys. J.* **2001**, *556*, 738–748. [[CrossRef](#)]
16. Jorstad, S.G.; Marscher, A.P.; Larionov, V.M.; Agudo, I.; Smith, P.S.; Gurwell, M.; Lähteenmäki, A.; Tornikoski, M.; Markowitz, A.; Arkharov, A.A.; et al. Flaring Behavior of the Quasar 3C 454.3 Across the Electromagnetic Spectrum. *Astrophys. J.* **2010**, *715*, 362–384. [[CrossRef](#)]
17. Marscher, A.P.; Jorstad, S.G.; Larionov, V.M.; Aller, M.F.; Aller, H.D.; Lähteenmäki, A.; Agudo, I.; Smith, P.S.; Gurwell, M.; Hagen-Thorn, V.A.; et al. Probing the Inner Jet of the Quasar PKS 1510-089 with Multi-Waveband Monitoring During Strong Gamma-Ray Activity. *Astrophys. J. Lett.* **2010**, *710*, L126–L131. [[CrossRef](#)]
18. Marscher, A.P.; Jorstad, S.G. The Megaparsec-scale X-ray Jet of The BL Lac Object OJ287. *Astrophys. J.* **2011**, *729*, 26. [[CrossRef](#)]
19. Schinzel, F.K.; Lobanov, A.P.; Taylor, G.B.; Jorstad, S.G.; Marscher, A.P.; Zensus, J.A. Relativistic outflow drives γ -ray emission in 3C 345. *Astron. Astrophys.* **2012**, *537*, A70. [[CrossRef](#)]
20. Rani, B.; Krichbaum, T.P.; Marscher, A.P.; Hodgson, J.A.; Fuhrmann, L.; Angelakis, E.; Britzen, S.; Zensus, J.A. Connection between inner jet kinematics and broadband flux variability in the BL Lacertae object S5 0716+714. *Astron. Astrophys.* **2015**, *578*, A123. [[CrossRef](#)]
21. Orienti, M.; Koyama, S.; D’Ammando, F.; Giroletti, M.; Kino, M.; Nagai, H.; Venturi, T.; Dallacasa, D.; Giovannini, G.; Angelakis, E.; et al. Radio and γ -ray follow-up of the exceptionally high-activity state of PKS 1510-089 in 2011. *Mon. Not. R. Astron. Soc.* **2013**, *428*, 2418–2429. [[CrossRef](#)]
22. Raiteri, C.M.; Villata, M.; D’Ammando, F.; Larionov, V.M.; Gurwell, M.A.; Mirzaqulov, D.O.; Smith, P.S.; Acosta-Pulido, J.A.; Agudo, I.; Arévalo, M.J.; et al. The awakening of BL Lacertae: observations by Fermi, Swift and the GASP-WEBT. *Mon. Not. R. Astron. Soc.* **2013**, *436*, 1530–1545. [[CrossRef](#)]
23. Ackermann, M.; Ajello, M.; Atwood, W.B.; Baldini, L.; Ballet, J.; Barbiellini, G.; Bastieri, D.; Becerra Gonzalez, J.; Bellazzini, R.; Bissaldi, E.; et al. The Third Catalog of Active Galactic Nuclei Detected by the Fermi Large Area Telescope. *Astrophys. J.* **2015**, *810*, 14. [[CrossRef](#)]
24. Rieger, F.M.; Levinson, A. Radio Galaxies at VHE energies. *arXiv* **2018**. Available online: <http://xxx.lanl.gov/abs/1810.05409> (accessed on 22 January 2019).
25. Wills, K.A.; Morganti, R.; Tadhunter, C.N.; Robinson, T.G.; Villar-Martin, M. Emission lines and optical continuum in low-luminosity radio galaxies. *Mon. Not. R. Astron. Soc.* **2004**, *347*, 771–786. [[CrossRef](#)]
26. Falomo, R.; Carangelo, N.; Treves, A. Host galaxies and black hole masses of low- and high-luminosity radio-loud active nuclei. *Mon. Not. R. Astron. Soc.* **2003**, *343*, 505–511. [[CrossRef](#)]
27. Lister, M.L.; Aller, M.F.; Aller, H.D.; Homan, D.C.; Kellermann, K.I.; Kovalev, Y.Y.; Pushkarev, A.B.; Richards, J.L.; Ros, E.; Savolainen, T. MOJAVE: XIII. Parsec-scale AGN Jet Kinematics Analysis Based on 19 years of VLBA Observations at 15 GHz. *Astron. J.* **2016**, *152*, 12. [[CrossRef](#)]

28. Mertens, F.; Lobanov, A.P.; Walker, R.C.; Hardee, P.E. Kinematics of the jet in M 87 on scales of 100–1000 Schwarzschild radii. *Astron. Astrophys.* **2016**, *595*, A54. [[CrossRef](#)]
29. Meyer, E.T.; Georganopoulos, M.; Sparks, W.B.; Perlman, E.; van der Marel, R.P.; Anderson, J.; Sohn, S.T.; Biretta, J.; Norman, C.; Chiaberge, M. A kiloparsec-scale internal shock collision in the jet of a nearby radio galaxy. *Nature* **2015**, *521*, 495–497. [[CrossRef](#)] [[PubMed](#)]
30. Harris, G.L.H.; Rejkuba, M.; Harris, W.E. The Distance to NGC 5128 (Centaurus A). *Publ. Astron. Soc. Aust.* **2010**, *27*, 457–462. [[CrossRef](#)]
31. Bettoni, D.; Falomo, R.; Fasano, G.; Govoni, F. The black hole mass of low redshift radiogalaxies. *Astron. Astrophys.* **2003**, *399*, 869–878. [[CrossRef](#)]
32. Bird, S.; Harris, W.E.; Blakeslee, J.P.; Flynn, C. The inner halo of M 87: A first direct view of the red-giant population. *Astron. Astrophys.* **2010**, *524*, A71. [[CrossRef](#)]
33. Walsh, J.L.; Barth, A.J.; Ho, L.C.; Sarzi, M. The M87 Black Hole Mass from Gas-dynamical Models of Space Telescope Imaging Spectrograph Observations. *Astrophys. J.* **2013**, *770*, 86. [[CrossRef](#)]
34. Strauss, M.A.; Huchra, J.P.; Davis, M.; Yahil, A.; Fisher, K.B.; Tonry, J. A redshift survey of IRAS galaxies. VII—The infrared and redshift data for the 1.936 Jansky sample. *Astrophys. J. Suppl. Ser.* **1992**, *83*, 29–63. [[CrossRef](#)]
35. Wilman, R.J.; Edge, A.C.; Johnstone, R.M. The nature of the molecular gas system in the core of NGC 1275. *Mon. Not. R. Astron. Soc.* **2005**, *359*, 755–764. [[CrossRef](#)]
36. Scharwächter, J.; McGregor, P.J.; Dopita, M.A.; Beck, T.L. Kinematics and excitation of the molecular hydrogen accretion disc in NGC 1275. *Mon. Not. R. Astron. Soc.* **2013**, *429*, 2315–2332. [[CrossRef](#)]
37. Bernardi, M.; Alonso, M.V.; da Costa, L.N.; Willmer, C.N.A.; Wegner, G.; Pellegrini, P.S.; Rité, C.; Maia, M.A.G. Redshift-Distance Survey of Early-Type Galaxies. I. The ENEARc Cluster Sample. *Astron. J.* **2002**, *123*, 2990–3017. [[CrossRef](#)]
38. Aleksić, J.; Ansoldi, S.; Antonelli, L.A.; Antoranz, P.; Babic, A.; Bangale, P.; Barrio, J.A.; González, J.B.; Bednarek, W.; Bernardini, E.; et al. Black hole lightning due to particle acceleration at subhorizon scales. *Science* **2014**, *346*, 1080–1084. [[CrossRef](#)]
39. Smith, R.J.; Lucey, J.R.; Hudson, M.J.; Schlegel, D.J.; Davies, R.L. Streaming motions of galaxy clusters within 12,000 kms⁻¹—I. New spectroscopic data. *Mon. Not. R. Astron. Soc.* **2000**, *313*, 469–490. [[CrossRef](#)]
40. van den Bosch, R.C.E. Unification of the fundamental plane and Super Massive Black Hole Masses. *Astrophys. J.* **2016**, *831*, 134. [[CrossRef](#)]
41. Jones, D.H.; Read, M.A.; Saunders, W.; Colless, M.; Jarrett, T.; Parker, Q.A.; Fairall, A.P.; Mauch, T.; Sadler, E.M.; Watson, F.G.; et al. The 6dF Galaxy Survey: Final redshift release (DR3) and southern large-scale structures. *Mon. Not. R. Astron. Soc.* **2009**, *399*, 683–698. [[CrossRef](#)]
42. Aharonian, F.; Akhperjanian, A.G.; Anton, G.; de Almeida, U.B.; Bazer-Bachi, A.R.; Becherini, Y.; Behera, B.; Benbow, W.; Bernlöhr, K.; Boisson, C.; et al. Discovery of Very High Energy γ -Ray Emission from Centaurus A with H.E.S.S. *Astrophys. J. Lett.* **2009**, *695*, L40–L44. [[CrossRef](#)]
43. Abdo, A.A.; Ackermann, M.; Ajello, M.; Atwood, W.B.; Baldini, L.; Ballet, J.; Barbiellini, G.; Bastieri, D.; Baughman, B.M.; Bechtol, K.; et al. Fermi Gamma-Ray Imaging of a Radio Galaxy. *Science* **2010**, *328*, 725.
44. Sahakyan, N.; Yang, R.; Aharonian, F.A.; Rieger, F.M. Evidence for a Second Component in the High-energy Core Emission from Centaurus A? *Astrophys. J. Lett.* **2013**, *770*, L6. [[CrossRef](#)]
45. Aharonian, F.; Akhperjanian, A.; Beilicke, M.; Bernlöhr, K.; Börst, H.G.; Bojahr, H.; Bolz, O.; Coarasa, T.; Contreras, J.L.; Cortina, J.; et al. Is the giant radio galaxy M 87 a TeV gamma-ray emitter? *Astron. Astrophys.* **2003**, *403*, L1–L5. [[CrossRef](#)]
46. Acciari, V.A.; Aliu, E.; Arlen, T.; Aune, T.; Beilicke, M.; Benbow, W.; Boltuch, D.; Bradbury, S.M.; Buckley, J.H.; Bugaev, V.; et al. Veritas 2008–2009 Monitoring of the Variable Gamma-ray Source M 87. *Astrophys. J.* **2010**, *716*, 819–824. [[CrossRef](#)]
47. Aleksić, J.; Alvarez, E.A.; Antonelli, L.A.; Antoranz, P.; Asensio, M.; Backes, M.; Barrio, J.A.; Bastieri, D.; Becerra González, J.; Bednarek, W.; et al. MAGIC observations of the giant radio galaxy M 87 in a low-emission state between 2005 and 2007. *Astron. Astrophys.* **2012**, *544*, A96. [[CrossRef](#)]
48. Aharonian, F.; Akhperjanian, A.G.; Bazer-Bachi, A.R.; Beilicke, M.; Benbow, W.; Berge, D.; Bernlöhr, K.; Boisson, C.; Bolz, O.; Borrel, V.; et al. Fast Variability of Tera-Electron Volt γ Rays from the Radio Galaxy M87. *Science* **2006**, *314*, 1424–1427. [[CrossRef](#)] [[PubMed](#)]

49. Beilicke, M.; VERITAS Collaboration. VERITAS Observations of M87 in 2011/2012. *AIP Conf. Proc.* **2012**, *1505*, 586–589.
50. Abdo, A.A.; Ackermann, M.; Ajello, M.; Asano, K.; Baldini, L.; Ballet, J.; Barbiellini, G.; Bastieri, D.; Baughman, B.M.; Bechtol, K.; et al. Fermi Discovery of Gamma-ray Emission from NGC 1275. *Astrophys. J.* **2009**, *699*, 31–39. [[CrossRef](#)]
51. Aleksić, J.; Alvarez, E.A.; Antonelli, L.A.; Antoranz, P.; Asensio, M.; Backes, M.; Barres de Almeida, U.; Barrio, J.A.; Bastieri, D.; Becerra González, J.; et al. Detection of very-high energy γ -ray emission from <ASTROBJ>NGC 1275</ASTROBJ> by the MAGIC telescopes. *Astron. Astrophys.* **2012**, *539*, L2.
52. Benbow, W.; VERITAS Collaboration. Highlights from the VERITAS AGN Observation Program. In Proceedings of the 34th International Cosmic Ray Conference (ICRC2015); The Hague, The Netherlands, 30 July–6 August 2015; Volume 34, p. 821.
53. Aleksić, J.; Antonelli, L.A.; Antoranz, P.; Backes, M.; Barrio, J.A.; Bastieri, D.; Becerra González, J.; Bednarek, W.; Berdyugin, A.; Berger, K.; et al. Detection of Very High Energy γ -ray Emission from the Perseus Cluster Head-Tail Galaxy IC 310 by the MAGIC Telescopes. *Astrophys. J. Lett.* **2010**, *723*, L207–L212. [[CrossRef](#)]
54. Mukherjee, R. VERITAS discovery of VHE emission from the FRI radio galaxy 3C 264. *Astronomer's Teleg. J.* **2018**, 11436.
55. Dyrda, M.; Wierzcholska, A.; Hervet, O.; Moderski, R.; Janiak, M.; Ostrowski, M.; Stawarz, Ł.; for the H. E. S. S. Collaboration. Discovery of VHE gamma-rays from the radio galaxy PKS 0625-354 with H.E.S.S. *ArXiv e-prints* **2015**, arXiv:1509.06851.
56. Fukazawa, Y.; Finke, J.; Stawarz, Ł.; Tanaka, Y.; Itoh, R.; Tokuda, S. Suzaku Observations of γ -Ray Bright Radio Galaxies: Origin of the X-Ray Emission and Broadband Modeling. *Astrophys. J.* **2015**, *798*, 74. [[CrossRef](#)]
57. Véron-Cetty, M.P.; Véron, P. A catalogue of quasars and active nuclei: 12th edition. *Astron. Astrophys.* **2006**, *455*, 773–777. [[CrossRef](#)]
58. Mueller, C.; Krauss, F.; Kadler, M.; Truedstedt, J.; Ojha, R.; Ros, E.; Wilms, J.; Boeck, M.; Dutka, M.; Carpenter, B. The TANAMI program: Southern-hemisphere AGN on (sub-)parsec scales. In Proceedings of the 11th European VLBI Network Symposium AMP Users Meeting, Bordeaux, France, 9–12 October 2012; p. 20.
59. Fanaroff, B.L.; Riley, J.M. The morphology of extragalactic radio sources of high and low luminosity. *Mon. Not. R. Astron. Soc.* **1974**, *167*, 31P–36P. [[CrossRef](#)]
60. Urry, C.M.; Padovani, P. Unified Schemes for Radio-Loud Active Galactic Nuclei. *Publ. Astron. Soc. Pac.* **1995**, *107*, 803. [[CrossRef](#)]
61. Hardcastle, M.J.; Evans, D.A.; Croston, J.H. The X-ray nuclei of intermediate-redshift radio sources. *Mon. Not. R. Astron. Soc.* **2006**, *370*, 1893–1904. [[CrossRef](#)]
62. Baum, S.A.; Zirbel, E.L.; O'Dea, C.P. Toward Understanding the Fanaroff-Riley Dichotomy in Radio Source Morphology and Power. *Astrophys. J.* **1995**, *451*, 88. [[CrossRef](#)]
63. Sikora, M.; Stawarz, Ł.; Lasota, J.P. Radio Loudness of Active Galactic Nuclei: Observational Facts and Theoretical Implications. *Astrophys. J.* **2007**, *658*, 815–828. [[CrossRef](#)]
64. Fabian, A.C.; Rees, M.J. The accretion luminosity of a massive black hole in an elliptical galaxy. *Mon. Not. R. Astron. Soc.* **1995**, *277*, L55–L58.
65. Asada, K.; Nakamura, M.; Doi, A.; Nagai, H.; Inoue, M. Discovery of Sub- to Superluminal Motions in the M87 Jet: An Implication of Acceleration from Sub-relativistic to Relativistic Speeds. *Astrophys. J. Lett.* **2014**, *781*, L2. [[CrossRef](#)]
66. Kovalev, Y.Y.; Lister, M.L.; Homan, D.C.; Kellermann, K.I. The Inner Jet of the Radio Galaxy M87. *Astrophys. J. Lett.* **2007**, *668*, L27–L30. [[CrossRef](#)]
67. Hada, K.; Park, J.H.; Kino, M.; Niinuma, K.; Sohn, B.W.; Ro, H.W.; Jung, T.; Algaba, J.C.; Zhao, G.Y.; Lee, S.S.; et al. Pilot KaVA monitoring on the M 87 jet: Confirming the inner jet structure and superluminal motions at sub-pc scales. *Publ. Astron. S. Jpn.* **2017**, *69*, 71. [[CrossRef](#)]
68. Walker, R.C.; Hardee, P.E.; Davies, F.B.; Ly, C.; Junor, W. The Structure and Dynamics of the Subparsec Jet in M87 Based on 50 VLBA Observations over 17 Years at 43 GHz. *Astrophys. J.* **2018**, *855*, 128. [[CrossRef](#)]
69. Biretta, J.A.; Junor, W. The Parsec-Scale Jet in M87. *Proc. Natl. Acad. Sci. USA* **1995**, *92*, 11364–11367. [[CrossRef](#)]

70. Meyer, E.T.; Sparks, W.B.; Biretta, J.A.; Anderson, J.; Sohn, S.T.; van der Marel, R.P.; Norman, C.; Nakamura, M. Optical Proper Motion Measurements of the M87 Jet: New Results from the Hubble Space Telescope. *Astrophys. J. Lett.* **2013**, *774*, L21. [[CrossRef](#)]
71. Giroletti, M.; Hada, K.; Giovannini, G.; Casadio, C.; Beilicke, M.; Cesarini, A.; Cheung, C.C.; Doi, A.; Krawczynski, H.; Kino, M.; et al. The kinematic of HST-1 in the jet of M 87. *Astron. Astrophys.* **2012**, *538*, L10. [[CrossRef](#)]
72. Müller, C.; Kadler, M.; Ojha, R.; Perucho, M.; Großberger, C.; Ros, E.; Wilms, J.; Blanchard, J.; Böck, M.; Carpenter, B.; et al. TANAMI monitoring of Centaurus A: The complex dynamics in the inner parsec of an extragalactic jet. *Astron. Astrophys.* **2014**, *569*, A115. [[CrossRef](#)]
73. Tingay, S.J.; Preston, R.A.; Jauncey, D.L. The Subparsec-Scale Structure and Evolution of Centaurus A. II. Continued Very Long Baseline Array Monitoring. *Astron. J.* **2001**, *122*, 1697–1706. [[CrossRef](#)]
74. Hardcastle, M.J.; Worrall, D.M.; Kraft, R.P.; Forman, W.R.; Jones, C.; Murray, S.S. Radio and X-Ray Observations of the Jet in Centaurus A. *Astrophys. J.* **2003**, *593*, 169–183. [[CrossRef](#)]
75. Marshall, H.L.; Miller, B.P.; Davis, D.S.; Perlman, E.S.; Wise, M.; Canizares, C.R.; Harris, D.E. A High-Resolution X-Ray Image of the Jet in M87. *Astrophys. J.* **2002**, *564*, 683–687. [[CrossRef](#)]
76. Lister, M.L.; Aller, M.F.; Aller, H.D.; Homan, D.C.; Kellermann, K.I.; Kovalev, Y.Y.; Pushkarev, A.B.; Richards, J.L.; Ros, E.; Savolainen, T. MOJAVE. X. Parsec-scale Jet Orientation Variations and Superluminal Motion in Active Galactic Nuclei. *Astron. J.* **2013**, *146*, 120. [[CrossRef](#)]
77. Dhawan, V.; Kellermann, K.I.; Romney, J.D. Kinematics of the Nucleus of NGC 1275 (3C 84). *Astrophys. J. Lett.* **1998**, *498*, L111–L114. [[CrossRef](#)]
78. Jorstad, S.G.; Marscher, A.P.; Morozova, D.A.; Troitsky, I.S.; Agudo, I.; Casadio, C.; Foord, A.; Gómez, J.L.; MacDonald, N.R.; Molina, S.N.; et al. Kinematics of Parsec-scale Jets of Gamma-Ray Blazars at 43 GHz within the VLBA-BU-BLAZAR Program. *Astrophys. J.* **2017**, *846*, 98. [[CrossRef](#)]
79. Kadler, M.; Eisenacher, D.; Ros, E.; Mannheim, K.; Elsässer, D.; Bach, U. The blazar-like radio structure of the TeV source IC 310. *Astron. Astrophys.* **2012**, *538*, L1. [[CrossRef](#)]
80. Giovannini, G.; Savolainen, T.; Orienti, M.; Nakamura, M.; Nagai, H.; Kino, M.; Giroletti, M.; Hada, K.; Bruni, G.; Kovalev, Y.Y.; et al. A wide and collimated radio jet in 3C84 on the scale of a few hundred gravitational radii. *Nat. Astron.* **2018**, *2*, 472–477. [[CrossRef](#)]
81. Kim, J.Y.; Krichbaum, T.P.; Lu, R.S.; Ros, E.; Bach, U.; Bremer, M.; de Vicente, P.; Lindqvist, M.; Zensus, J.A. The limb-brightened jet of M87 down to the 7 Schwarzschild radii scale. *Astron. Astrophys.* **2018**, *616*, A188. [[CrossRef](#)]
82. Boccardi, B.; Krichbaum, T.P.; Ros, E.; Zensus, J.A. Radio observations of active galactic nuclei with mm-VLBI. *Astron. Astrophys. Rev.* **2017**, *25*, 4. [[CrossRef](#)]
83. Hada, K.; Doi, A.; Kino, M.; Nagai, H.; Hagiwara, Y.; Kawaguchi, N. An origin of the radio jet in M87 at the location of the central black hole. *Nature* **2011**, *477*, 185–187. [[CrossRef](#)] [[PubMed](#)]
84. Doeleman, S.S.; Fish, V.L.; Schenck, D.E.; Beaudoin, C.; Blundell, R.; Bower, G.C.; Broderick, A.E.; Chamberlin, R.; Freund, R.; Friberg, P.; et al. Jet-Launching Structure Resolved Near the Supermassive Black Hole in M87. *Science* **2012**, *338*, 355. [[CrossRef](#)] [[PubMed](#)]
85. Hada, K.; Kino, M.; Doi, A.; Nagai, H.; Honma, M.; Akiyama, K.; Tazaki, F.; Lico, R.; Giroletti, M.; Giovannini, G.; et al. High-sensitivity 86 GHz (3.5 mm) VLBI Observations of M87: Deep Imaging of the Jet Base at a Resolution of 10 Schwarzschild Radii. *Astrophys. J.* **2016**, *817*, 131. [[CrossRef](#)]
86. Lu, R.S.; Broderick, A.E.; Baron, F.; Monnier, J.D.; Fish, V.L.; Doeleman, S.S.; Pankratius, V. Imaging the Supermassive Black Hole Shadow and Jet Base of M87 with the Event Horizon Telescope. *Astrophys. J.* **2014**, *788*, 120. [[CrossRef](#)]
87. Rani1, B.; Jorstad, S.G.; Marscher, A.P.; Agudo, I.; Sokolovsky, K.V.; Larionov, V.M.; Smith, P.; Mosunova, D.A.; Borman, G.A.; Grishina, T.S. Exploring the connection between parsec-scale jet activity and broadband outbursts in 3C 279. *Astrophys. J.* **2018**, *858*, 80. [[CrossRef](#)]
88. Marscher, A.P.; Jorstad, S.G.; D’Arcangelo, F.D.; Smith, P.S.; Williams, G.G.; Larionov, V.M.; Oh, H.; Olmstead, A.R.; Aller, M.F.; Aller, H.D.; et al. The inner jet of an active galactic nucleus as revealed by a radio-to- γ -ray outburst. *Nature* **2008**, *452*, 966–969. [[CrossRef](#)]
89. Lott, B.; Escande, L.; Larsson, S.; Ballet, J. An adaptive-binning method for generating constant-uncertainty/constant-significance light curves with Fermi-LAT data. *Astron. Astrophys.* **2012**, *544*, A6. [[CrossRef](#)]

90. Albert, J.; Aliu, E.; Anderhub, H.; Antoranz, P.; Armada, A.; Baixeras, C.; Barrio, J.A.; Bartko, H.; Bastieri, D.; Becker, J.K.; et al. Variable Very High Energy γ -Ray Emission from Markarian 501. *Astrophys. J.* **2007**, *669*, 862–883. [[CrossRef](#)]
91. Hada, K.; Kino, M.; Nagai, H.; Doi, A.; Hagiwara, Y.; Honma, M.; Giroletti, M.; Giovannini, G.; Kawaguchi, N. VLBI Observations of the Jet in M 87 during the Very High Energy γ -Ray Flare in 2010 April. *Astrophys. J.* **2012**, *760*, 52. [[CrossRef](#)]
92. Hada, K.; Giroletti, M.; Kino, M.; Giovannini, G.; D'Ammando, F.; Cheung, C.C.; Beilicke, M.; Nagai, H.; Doi, A.; Akiyama, K.; et al. A Strong Radio Brightening at the Jet Base of M 87 during the Elevated Very High Energy Gamma-Ray State in 2012. *Astrophys. J.* **2014**, *788*, 165. [[CrossRef](#)]
93. Marscher, A.P.; Gear, W.K. Models for high-frequency radio outbursts in extragalactic sources, with application to the early 1983 millimeter-to-infrared flare of 3C 273. *Astrophys. J.* **1985**, *298*, 114–127. [[CrossRef](#)]
94. Chidiac, C.; Rani, B.; Krichbaum, T.P.; Angelakis, E.; Fuhrmann, L.; Nestoras, I.; Zensus, J.A.; Sievers, A.; Ungerechts, H.; Itoh, R.; et al. Exploring the nature of the broadband variability in the flat spectrum radio quasar 3C 273. *Astron. Astrophys.* **2016**, *590*, A61. [[CrossRef](#)]
95. Hodgson, J.A.; Krichbaum, T.P.; Marscher, A.P.; Jorstad, S.G.; Rani, B.; Marti-Vidal, I.; Bach, U.; Sanchez, S.; Bremer, M.; Lindqvist, M.; et al. Location of γ -ray emission and magnetic field strengths in OJ 287. *Astron. Astrophys.* **2017**, *597*, A80. [[CrossRef](#)]
96. Karamanavis, V.; Fuhrmann, L.; Angelakis, E.; Nestoras, I.; Myserlis, I.; Krichbaum, T.P.; Zensus, J.A.; Ungerechts, H.; Sievers, A.; Gurwell, M.A. What can the 2008/10 broadband flare of PKS 1502+106 tell us? Nuclear opacity, magnetic fields, and the location of γ rays. *Astron. Astrophys.* **2016**, *590*, A48. [[CrossRef](#)]
97. Aharonian, F.; Akhperjanian, A.G.; Bazer-Bachi, A.R.; Behera, B.; Beilicke, M.; Benbow, W.; Berge, D.; Bernlöhner, K.; Boisson, C.; Bolz, O.; et al. An Exceptional Very High Energy Gamma-Ray Flare of PKS 2155-304. *Astrophys. J. Lett.* **2007**, *664*, L71–L74. [[CrossRef](#)]
98. Zhang, H.; Li, X.; Guo, F.; Giannios, D. Large-amplitude Blazar Polarization Angle Swing as a Signature of Magnetic Reconnection. *Astrophys. J. Lett.* **2018**, *862*, L25. [[CrossRef](#)]
99. Petropoulou, M.; Giannios, D.; Sironi, L. Blazar flares powered by plasmoids in relativistic reconnection. *Mon. Not. R. Astron. Soc.* **2016**, *462*, 3325–3343. [[CrossRef](#)]
100. Giannios, D. Reconnection-driven plasmoids in blazars: Fast flares on a slow envelope. *Mon. Not. R. Astron. Soc.* **2013**, *431*, 355–363. [[CrossRef](#)]
101. Petropoulou, M.; Sironi, L. The Steady Growth of the High-Energy Spectral Cutoff in Relativistic Magnetic Reconnection. *Mon. Not. Roy. Astron. Soc.* **2018**, *481*, 4. [[CrossRef](#)]
102. Kagan, D.; Sironi, L.; Cerutti, B.; Giannios, D. Relativistic Magnetic Reconnection in Pair Plasmas and Its Astrophysical Applications. *Space Sci. Rev.* **2015**, *191*, 545–573. [[CrossRef](#)]
103. Hirovani, K.; Pu, H.Y. Energetic Gamma Radiation from Rapidly Rotating Black Holes. *Astrophys. J.* **2016**, *818*, 50. [[CrossRef](#)]
104. Rieger, F.M. Nonthermal Processes in Black Hole-Jet Magnetospheres. *Int. J. Modern Phys. D* **2011**, *20*, 1547–1596. [[CrossRef](#)]
105. Blandford, R.D.; Znajek, R.L. Electromagnetic extraction of energy from Kerr black holes. *Mon. Not. R. Astron. Soc.* **1977**, *179*, 433–456. [[CrossRef](#)]
106. Katsoulakos, G.; Rieger, F.M. Magnetospheric Gamma-Ray Emission in Active Galactic Nuclei. *Astrophys. J.* **2018**, *852*, 112. [[CrossRef](#)]
107. Blandford, R.; Yuan, Y.; Hoshino, M.; Sironi, L. Magnetoluminescence. *Space Sci. Rev.* **2017**, *207*, 291–317. [[CrossRef](#)]
108. Blandford, R.; East, W.; Nalewajko, K.; Yuan, Y.; Zrake, J. Active Galactic Nuclei: The TeV Challenge. *arXiv* **2015**, arXiv:1511.07515.
109. McKinney, J.C.; Tchekhovskoy, A.; Blandford, R.D. Alignment of Magnetized Accretion Disks and Relativistic Jets with Spinning Black Holes. *Science* **2013**, *339*, 49. [[CrossRef](#)] [[PubMed](#)]
110. Zamaninasab, M.; Clausen-Brown, E.; Savolainen, T.; Tchekhovskoy, A. Dynamically important magnetic fields near accreting supermassive black holes. *Nature* **2014**, *510*, 126–128. [[CrossRef](#)] [[PubMed](#)]
111. Liska, M.; Hesp, C.; Tchekhovskoy, A.; Ingram, A.; van der Klis, M.; Markoff, S. Formation of precessing jets by tilted black hole discs in 3D general relativistic MHD simulations. *Mon. Not. R. Astron. Soc.* **2018**, *474*, L81–L85. [[CrossRef](#)]

112. Zhang, H.; Li, H.; Guo, F.; Taylor, G. Polarization Signatures of Kink Instabilities in the Blazar Emission Region from Relativistic Magnetohydrodynamic Simulations. *Astrophys. J.* **2017**, *835*, 125. [[CrossRef](#)]
113. Marscher, A.P. Turbulent, Extreme Multi-zone Model for Simulating Flux and Polarization Variability in Blazars. *Astrophys. J.* **2014**, *780*, 87. [[CrossRef](#)]
114. Acharya, B.S.; Agudo, I.; Al Samarai, I.; Alfaro, R.; Alfaro, J.; Alispach, C.; Alves Batista, R.; Amans, J.P.; Amato, E.; Ambrosi, G.; et al. Science with the Cherenkov Telescope Array. *arXiv* **2017**, arXiv:1709.07997.
115. IceCube Collaboration; Aartsen, M.G.; Ackermann, M.; Adams, J.; Aguilar, J.A.; Ahlers, M.; Ahrens, M.; Al Samarai, I.; Altmann, D.; Andeen, K.; et al. Multimessenger observations of a flaring blazar coincident with high-energy neutrino IceCube-170922A. *Science* **2018**, *361*, eaat1378.



© 2019 by the authors. Licensee MDPI, Basel, Switzerland. This article is an open access article distributed under the terms and conditions of the Creative Commons Attribution (CC BY) license (<http://creativecommons.org/licenses/by/4.0/>).